

Topical Application of *Paraboea leuserensis* on Excision Wound with Angiogenesis and Vascular Endothelial Growth Factor Analysis

Dyah Wijiana Heryani¹, Fiska Maya Wardhani¹, Yensuari², Nadya Nazimuddin Putri², Leo Nardi², Refi Ikhtiari^{1*}

¹Department of Biomedical Sciences, Faculty of Medicine, Universitas Prima Indonesia, Medan 20118, Indonesia

²Department of Medicine, Faculty of Medicine, Universitas Prima Indonesia, Medan 20118, Indonesia

ARTICLE INFO

Article history:

Received May 15, 2023

Received in revised form October 1, 2023

Accepted November 1, 2023

KEYWORDS:

Angiogenesis,
Antibacterial effect,
P. leuserensis,
VEGF,
Wound healing

ABSTRACT

Gagatan harimau or *Paraboea leuserensis* B.L. Burtt is an endemic plant that grows in limestone areas, natively found in Leuser Mountain Area, North Sumatra Province, Indonesia. This study determines the wound healing potential of *P. leuserensis* gel-based ethanolic extract (PGEE) on full-thickness excision wounds based on the angiogenesis and VEGF expression. Here, we reported 67 compounds detected by LC-MS/MS from the ethanolic extract. The antibacterial activity regarding pathogenic wound infection was also investigated. The experimental study used 30 *Rattus novergicus*, randomly divided into five treatment groups: base gel as a negative control, Bioplacenton as a positive control, PGEE 2.5%, 5%, and 10%. Experimental data showed that PGEE indicated a significant effect on bacterial inhibition ($p = 0.02$), where the greatest inhibitory was found against *S. epidermidis*. Topical application of PGEE showed significant differences in the number of blood vessels of PGEE 2.5% and 10% ($p = 0.007$) and expression of VEGF ($p < 0.05$). The correlation between the number of blood vessels and VEGF was also described with the number of macrophages, fibroblasts, collagen, and wound diameter. Overall, this study demonstrates the pharmacological potential of PGEE for wound healing applications regarding angiogenesis and VEGF expression.

1. Introduction

Paraboea leuserensis B.L. Burtt has common local name as "Gagatan Harimau" in North Sumatra Province, Indonesia. *P. leuserensis* was grown in the forest's interior, on the edge of a steep ravine or valley, and on limestone rocks or karst. Local people said that wild tigers like to eat leaves of *P. leuserensis* after eating their prey, presumably as an antitoxin. *P. leuserensis* has been used traditionally by residents as herbal medicine or "jamu" for treating colic, high fever, and wound healing. Previous studies reported that *Paraboea* plants leaves have several activities, including anti-inflammatory, antibacterial, and antioxidant, which have the main content of flavonoids such as myricetin, myricitrin, quercetin, kaempferol, and ellagic acid (Wang *et al.* 2011; Gong *et al.* 2019; Fu *et al.* 2022; Nanjala *et al.* 2022).

Recently, there has been no scientific literature regarding the wound-healing effects of *P. leuserensis*. On the other hand, there is a rising public interest in using natural-based health products for wound treatment. Thus, we are interested in exploring the wound-healing effects of *P. leuserensis* in the context of angiogenesis and VEGF expression analysis.

Angiogenesis is a critical process in wound healing, allowing for the formation of new blood vessels in the injured tissue, which provides essential nutrients and oxygen to support tissue growth and repair (Raina *et al.* 2021). The angiogenesis process involves releasing growth factors, such as vascular endothelial growth factor (VEGF), that stimulate the growth of new blood vessels. The VEGF has functioned to form new blood vessels produced by various types of cells, such as macrophages, fibroblasts, and endothelial cells (Wise *et al.* 2018). Furthermore, the wound healing process includes several synergistic and overlapping phases, including homeostasis, inflammation, proliferation, and remodeling (Maruf *et al.* 2021).

* Corresponding Author

E-mail Address: refiikhtiari@unprimdn.ac.id

In addition, microbial invasion might be the most common type of wound infection that interferes with wound healing. Gram-positive bacteria such as *Staphylococcus aureus* may play a major role in the first stage of infection, and gram-negative bacteria such as *Escherichia coli* and *Pseudomonas aeruginosa* can be found when the chronic wound has been developed (Moeini *et al.* 2020). Therefore, in this research, we also consider the antibacterial effect of PGEE regarding wound infection.

In this study, the wound healing activity of *P. leuserensis* leaves in the formulation of a gel-based ethanolic extract has been investigated based on the antibacterials effects as well as angiogenesis aspects such as number of macrophage cells, fibroblast cells, collagen density, number of blood vessels, and VEGF expression as a biomarker of the wound healing process. This research aims to reveal the wound healing and antibacterial effects of *P. leuserensis* gel extract on the excision wound from angiogenesis and VEGF expression perspectives.

2. Materials and Methods

2.1. Materials

The *Paraboea leuserensis* B.L. Burt were collected from the rain forest of Gunung Leuser, Bahorok District, Langkat Regency, North Sumatra Province, Indonesia. Herbarium Bogoriense conducted identification of plant species with No. B-1808/ II.6.2/DI.05.07/6/2022. Fresh leaves were washed under running water until clean, drained, and weighed. Then, it was dried in a drying cabinet at $\pm 40^{\circ}\text{C}$. The dried sample was then blended into powder and stored in a dry container at room temperature.

2.2. Sample Preparation of PGEE

About 1,045 g of dried leaves were macerated by ethanol 96% for five days, followed by rotary evaporation at $\pm 40^{\circ}\text{C}$ to get the crude extract. After that, about 5 g of each *Simplicia* was determined for water content, water-soluble content, ethanol-soluble content, total ash content, and acid-insoluble ash content (Depkes RI 2016). The formulation of PGEE in the Base gel was varied into 2.5, 5, and 10% (w/v). Then, a cycling test was conducted to evaluate the stability of PGEE formulae, including organoleptic, homogeneity, viscosity, pH, and spreadability (Sara and Rosiana 2021).

2.3. Phytochemistry Analysis

Preliminary screening of flavonoids, saponins, tannins, alkaloids, glycosides, and steroid contents referred to the established protocol (Farnsworth 1966; Ditjen POM 2000; Depkes RI 2016). LC-MS/MS analyzed further analysis on the bioactive compounds at Primkoppol Puslabfor POLRI Jakarta Selatan No.12/Inv/Primkoppol/IX/2022.

2.4. In Vitro Analysis of the Antibacterial Effect

The disc diffusion method was used by measuring the diameter of the inhibition zone of bacterial growth against the most active bacteria on the *P. leuserensis* extract. The bacteria used in this experiment were *S. aureus*, *S. epidermidis*, and *P. aeruginosa*. The protocol referred to previous studies using the disc diffusion method, where 0.1 bacteria suspension was inoculated in Muller Hinton Agar media. The inhibition zone was calculated by measuring the clear zone around the paper disc (Puguh Surjowardojo and Tri Eko Susilorini 2015; Nurhayati *et al.* 2020; Winastri *et al.* 2020).

2.5. In Vivo Analysis of Wound Healing Effect

The animal model was 30 individuals of white male *Rattus norvegicus*, aged 3 months, weighing 150–230 grams, who had been acclimatized for 7 days. Wistar rats were divided into 6 individuals per group (negative control, positive control, PGEE 2.5%, 5%, and 10%). Ethical clearance was issued by Komite Etik Penelitian Kesehatan (KEPK) Universitas Prima Indonesia No. 013/KEPK/UNPRI/VII/2022. After acclimatization, the Wistar rats were anesthetized with 0.2 cc of Ketamin-hameln[®] and injured on the dorsal side of the body with a round incision using a 2 × 2 cm blade. Then we applied the Base gel (negative control), Bioplacenton[®] (positive control), PGEE 2.5%, 5%, and 10%. The wound healing effect was evaluated by measuring the wound diameter on days 0, 6, and 12. Observation on the wound healing process was counted by percentage (Wulandari *et al.* 2021; Winarni *et al.* 2022). On the 12th day, the Wistar rats were terminated, and the wound tissue was taken, which was fixed with 10% NBF and then stained with HE. After that, we counted the number of macrophages, fibroblasts, collagen density, and blood vessels (Suvarna *et al.* 2019; Sunarto *et al.* 2020). Moreover, immunohistochemical staining with HE was performed to evaluate VEGF expression with IRS scores. The Immunoreactive Score (IRS) is a scoring

system commonly used to evaluate the expression and distribution of specific proteins or markers in tissue sections using immunohistochemistry (Su *et al.* 2019; Sunariani *et al.* 2020; Sunarto *et al.* 2020).

2.6. Statistical Analysis

The collected data were processed with SPSS version 26. Then, we analyzed the mean, standard deviation, normality of distribution with Shapiro-Wilk, and homogeneity with Levene's test. For comparison, we used a parametric statistical test. If the data curve is normally distributed and homogeneous with one-way ANOVA, then we applied the Tukey Post LSD to see the different effects of each treatment. However, if the data curve is skewed, not normally distributed, or homogeneous, we used the Kruskal-Wallis as the non-parametric statistical test followed by the Mann-Whitney U test (Purnomo and Syamsul 2012).

3. Results

3.1. Identification of Plant Species

Leaves of gagatan harimau or *Paraboea leuserensis* B.L. Burtt belong to the family of Gesneriaceae. The stature was perennial herbs with leaves like stacked roses (perennial rosulate herb). The leaf surface morphology was dark green, smooth, matte brown indumentum, slightly oval or obovate. Short flower size or equal to the leaves, little or no flowering. *P. leuserensis* is usually found in karst limestone areas on the edge of forest ravines and is difficult to breed in the common humus media. The plant images of *P. leuserensis* can be seen in the Supplementary Figure 1.

3.2. Physical Characteristics of PGEE

After the extraction process, we obtained 121 g crude extract from 1,045 g *Simplicia* with a water content of 18.56%, water-soluble content of 26.59%, ethanol-soluble content of 41.36%, total ash content of 3.48%, as well as acid insoluble ash content 0.7%. After six cycles of stability observation (12 days), we found that PGEE 2.5%, 5%, and 10% have a unique odor, dark green color, homogenous in thick gel, and no organoleptic changes. There were slight changes in viscosity, pH, and spreadability after 12 d, but all these changes were insignificant. The data of physical characteristics of PGEE was shown in the Supplementary Table 1. The images of *P. leuserensis* in crude extract and the gel-based forms were presented in the Supplementary Figure 2.

3.3. Phytochemistry Analysis

Preliminary screening of phytochemistry analysis showed that the ethanolic extract of *P. leuserensis* leaves contained flavonoids, saponins, tannins, alkaloids, glycosides, and steroids. In in-depth analysis with LC-MS, we reported 67 metabolite compounds, which may be correlated with the wound healing mechanism, such as betaine, myricetin, luteolin-7-O-glycosides, myricitrin, ellagic acid, quercitrin, curcumin, kaempferol, quercetin, linoleic acid, hydroxycinnamic acid, arginine, proline, etc. The LC-MS data of metabolite compounds were available in the Supplementary Table 2.

3.4. In Vitro Analysis of the Antibacterial Effect

We obtained positive results by measuring the diameter of the inhibition zone of bacterial growth against *S. aureus*, *S. epidermidis*, and *P. aeruginosa*. The formation of an inhibition zone around the paper disc demonstrated strong inhibition activity. The diameter of the inhibition zone ranged from 10.4 to 13 mm in the following order: *S. epidermidis* > *S. aureus* > *P. aeruginosa*. These results indicate that PGEE is categorized as a strong inhibition of the bacterial growth of *S. epidermidis*. The average diameter of the inhibition zone was presented in Figure 1, and the disc diffusion images were available in the Supplementary Figure 3. Statistic analyses with Saphiro-Wilk showed that all data were normally distributed ($p > 0.05$), but Levene's test indicated that data was not homogenous ($p < 0.05$). Then, the Kruskal-Wallis and Mann-Whitney U tests showed significant differences in the inhibition zone among groups ($p < 0.05$).

3.5. In Vivo Analysis of Wound Healing Effect

3.5.1. Wound Diameter

On average, the Bioplacenton wound diameter was seen to be flatter and constantly decreasing than the other groups in 0, 6, and 12 days. While the PGEE 10% experienced a significant decrease in wound diameter, followed by 2.5% and 5%. We observed that the diameter of the dorsal skin wound in male rats decreased every 2 days until the 12th day. The mean wound diameter is shown in Figure 2A, and the percentage of wound healing is presented in Figure 2B. Statistic analyses showed that all data were normally distributed ($p > 0.05$) and homogenous ($p > 0.05$). Further analysis with ANOVA and followed by Tukey Post LSD test showed that there were no

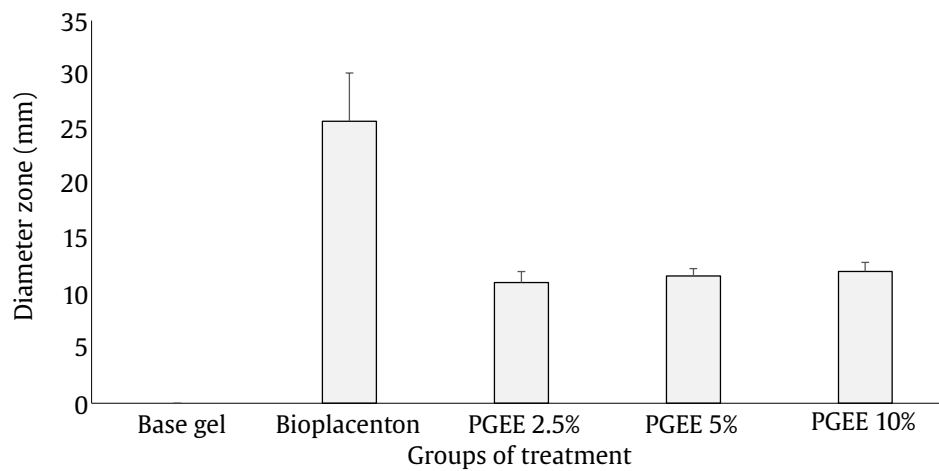


Figure 1. The average diameter of the inhibition zone (mm). Error bars represent the standard of error

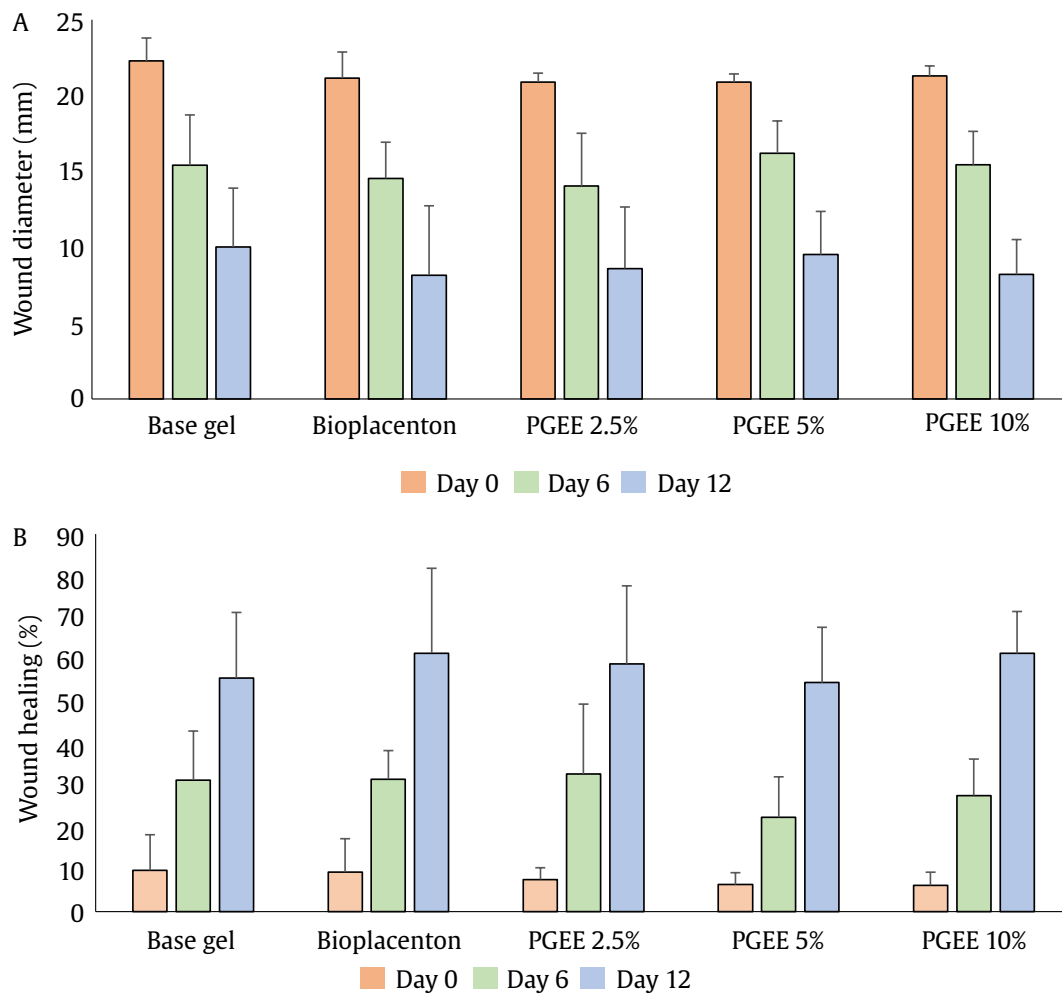


Figure 2. (A) The average of wound diameter and (B) percentage of wound healing. Error bars represent the standard of error

significant differences in wound healing among groups ($p>0.05$). In clinical appearance, the rats' wounds started to close after days 1, 6, and 12. Additionally, we observed that the wounds were clean without any other dirty exudates.

3.5.2. Number of Macrophages

The mean results of the number of macrophages from the highest to the lowest were PGEE 5%, PGEE 2.5%, Base gel, PGEE 10%, and Bioplacenton, respectively, as shown in Figure 3. The Bioplacenton group had the lowest number of macrophages compared to the other groups, whereas the PGEE 5% has the highest number. Statistics analyses showed that the number of macrophages was normally distributed ($p>0.05$) and not homogenous ($p<0.05$). Further analysis with the Kruskal Wallis test ($p>0.05$) and followed by the Mann-Whitney U test ($p>0.05$) have shown that there were no significant differences in macrophage number among groups. The microscopic micrograph of HE-stained macrophages at 400×5 visual fields is shown in Table 1.

3.5.3. Number of Fibroblasts

The mean number of fibroblasts from the highest to the lowest were Base gel, Bioplacenton, PGEE 5%, PGEE 10%, and PGEE 2.5%, respectively, as shown in Figure 4. Statistics analyses showed that the number of fibroblasts was not normally distributed ($p<0.05$) but homogenous ($p>0.05$). Further analysis with the Kruskal Wallis test ($p>0.05$) and followed by the Mann-Whitney U test ($p>0.05$) have shown that there were no significant differences in fibroblasts among groups. The microscopic micrograph of HE-

stained fibroblasts at 400×5 visual fields is shown in Table 1.

3.5.4. Number of Blood Vessels

The number of blood vessels from the highest to the lowest was PGEE 2.5%, Base gel, PGEE 5%, Bioplacenton, and PGEE 10%, respectively, as shown in Figure 5. Statistics analyses showed that the number of blood vessels was normally distributed ($p>0.05$) and homogenous ($p>0.05$). ANOVA showed no significant difference in PGEE application ($p>0.05$). Further analysis with the Tukey Post LSD test showed there were no significant differences in wound healing among groups ($p>0.05$) except between PGEE 2.5% and PGEE 10% ($p<0.05$). The microscopic micrograph of HE-stained blood vessels at 400×5 visual fields is available in Table 1.

3.5.5. Collagen Density

The collagen density scores from the highest to the lowest were Bioplacenton, PGEE 5%, PGEE 10%, PGEE 2.5%, and Base gel, respectively, as shown in Figure 6. Statistics analyses showed that data was not normally distributed ($p<0.05$) and not homogenous ($p<0.05$). Further analysis with the Kruskal Wallis test ($p>0.05$) and followed by the Mann-Whitney U test ($p>0.05$) have shown that there were no significant differences in collagen density among groups. The microscopic micrograph of HE-stained collagen density s at 400×5 visual fields, as shown in Table 1.

3.5.6. VEGF Expression

Microscopic examination of wounds stained with VEGF-A antibodies on day 12 showed that

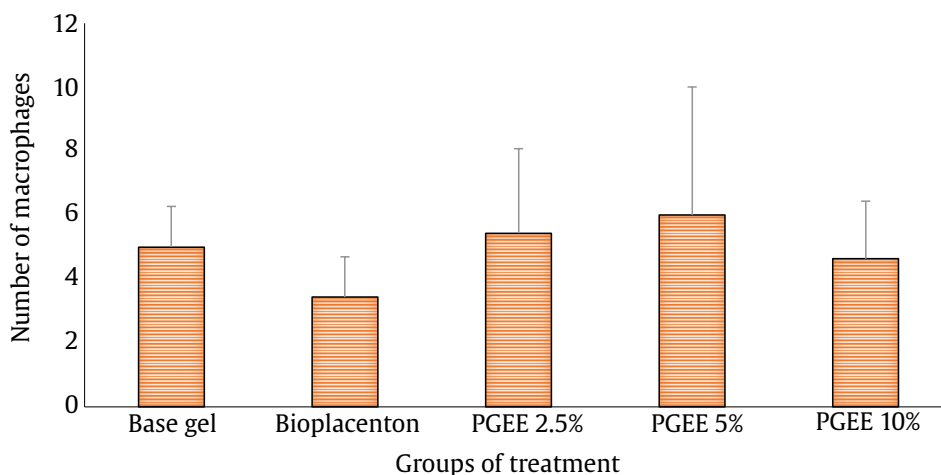
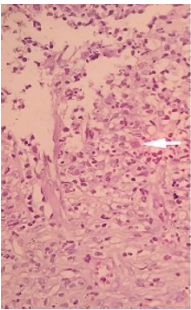
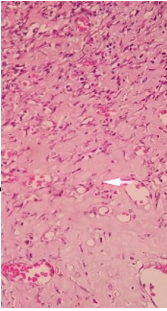
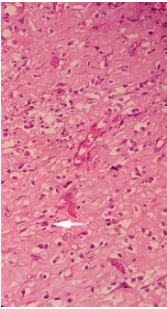
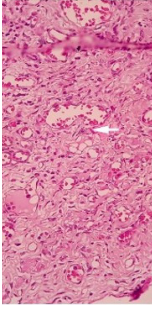
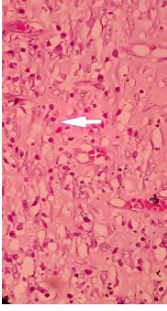
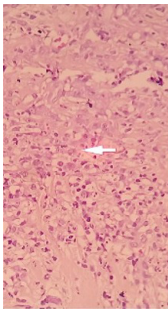
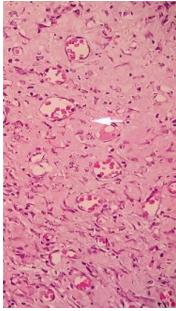
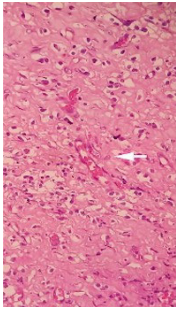
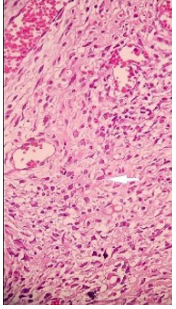
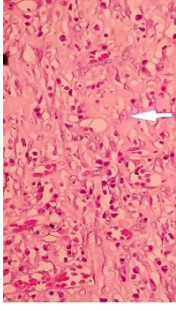
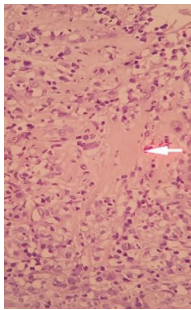
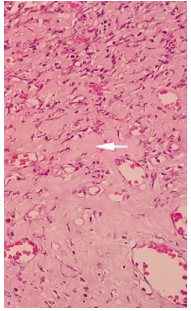
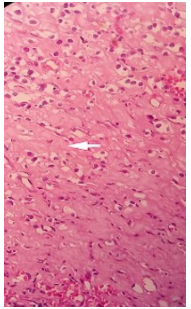
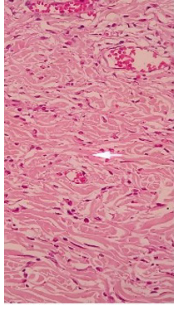
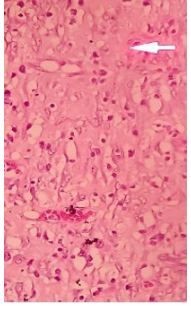
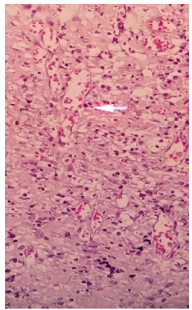
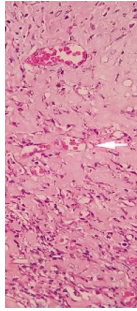
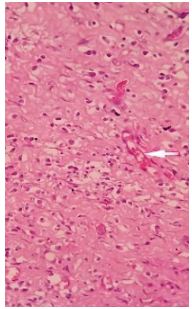
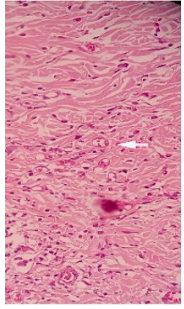
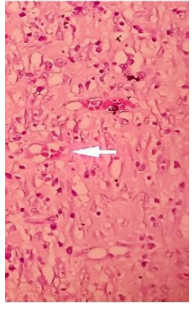
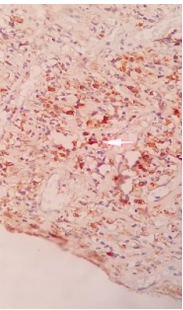
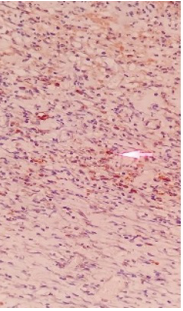
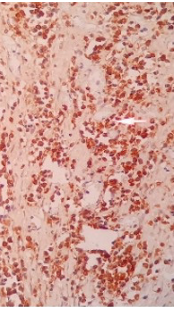
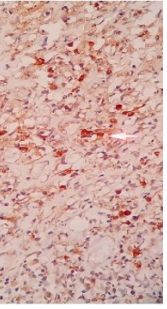
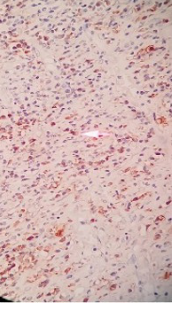


Figure 3. The average number of macrophages after 12 days of treatment. Error bars represent the standard of error

Table 1. The micrograph of HE-stained macrophages, fibroblasts, collagen, blood vessels, and VEGF expression at 400 × 5 visual fields. The white arrows showed each parameter

	Gel-basis	Bioplacenton	PGEE 2.5%	PGEE 5%	PGEE 10%
Macrophages					
Fibroblast					
Collagen					
Blood vassels					
VEGF expression					

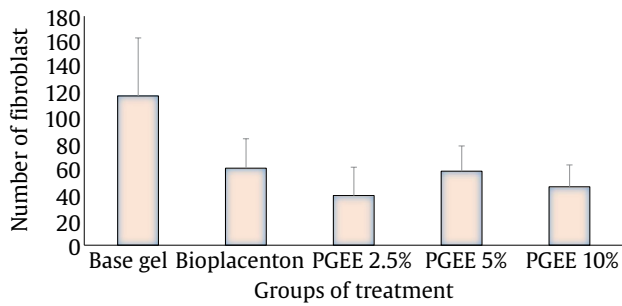


Figure 4. The average number of fibroblasts after 12 days of treatment. Error bars represent the standard of error

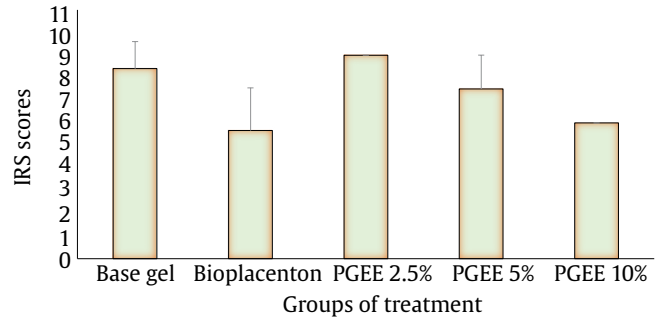


Figure 7. The average of IRS scores after 12 days of treatment. Error bars represent the standard of error

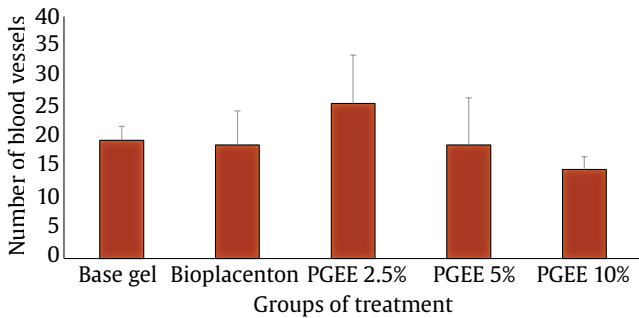


Figure 5. The average number of blood vessels after 12 days of treatment. Error bars represent the standard of error

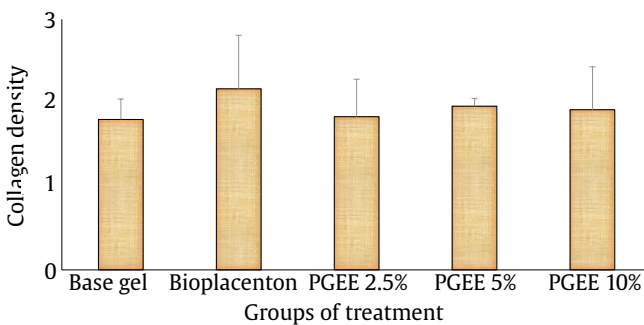


Figure 6. The average of collagen density after 12 days of treatment. Error bars represent the standard of error

Bioplacenton, PGEE 5% and PGEE 10% had moderate VEGF expression in the vascular endothelial cells. Interestingly, the Base gel and PGEE 2.5% indicated that VEGF was highly expressed in vascular endothelial cells, fibroblast cells, and epithelial cells. The microscopic micrograph of HE stained in Table 1 illustrated that the decreased or low expression of VEGF between Bioplacenton and PGEE 10% is not much different.

The IRS scores presented in Figure 7 have indicated that the lowest VEGF expression was found in the Bioplacenton group, followed by PGEE 10%.

Statistically, the IRS score was normally distributed ($p > 0.05$) but not homogeneous ($p < 0.05$). Then, the Kruskal Wallis test has sig 0.004 ($p < 0.05$), meaning that there was a significant effect of PGEE on the VEGF expression in rat skin excision wound tissue. These results were in line with the theory of wound healing that VEGF expression started to decrease at the beginning of the remodeling phase (after 12 days).

Based on the data obtained, this study has proved the effect of topical administration of PGEE on inducing the angiogenesis process and the remodeling or maturation stage on full-thickness excision wound healing in male Wistar rats. The effects were reported in the form of reduced wound diameter, increased percentage of wound healing, decreased macrophages, decreased fibroblasts, increased collagen density, decreased number of blood vessels, and decreased VEGF expression.

4. Discussion

This research reveals how *P. leuserensis* gel-based ethanolic extract (PGEE) affects the angiogenesis process, and the remodeling wound healing process will be discussed here. The analysis will be described consecutively by the feasibility test of the PGEE product as well as its effect on the reduced wound diameter, increased percentage of wound healing, decreased macrophages, decreased fibroblasts, increased collagen density, decreased number of blood vessels, decreased VEGF expression will be discussed based on the presented results.

The as-prepared *P. leuserensis* gel-based ethanolic extract (PGEE) has a unique odor, dark green color, and thick homogenous gel. The lower pH and viscosity found in the higher concentration are associated with more contents of metabolites (Aji and Rubiyanti 2021).

However, the pH range of 4.5-6.5 was acceptable and biocompatible with the topical skin application (Harahap 2017). However, slight changes in viscosity, pH, and spreadability after six cycles have not degraded the physical quality of PGEE at any concentration (Supplementary Table 1). Physical characteristics of PGEE showed the potential for medicinal preparation in the future.

Secondary metabolites of the PGEE may play a role in the wound-healing process. To our knowledge, this study is the first report on the phytochemical contents of *P. leuserensis* extract based on LC-MS/MS data analysis (Fu *et al.* 2022). From the 67 metabolites compounds detected from *P. leuserensis* extract (Supplementary Table 2), we highlighted the presence of betaine, myricetin, luteolin-7-O-glycosides, myricitrin, ellagic acid, quercitrin, curcumin, kaempferol, quercetin, linoleic acid, hydroxycinnamic acid, arginine, and proline as the bioactive compounds that having contributions to the wound healing process (Shah and Amini-Nik 2017). Based on the literature, those bioactive compounds were reported to have anti-inflammation by radical scavenging via xanthine oxidase and anti-thrombogenic (Panche *et al.* 2016). Several compounds of *Parabosides* groups have been isolated from *Paraboea martinii* L. Burt and showed protection effects on the PC12 cell damages induced by peroxidase (Wang *et al.* 2011; Gong *et al.* 2019). Tannin groups have also been reported for re-epithelization, stabilizing collagen and elastin in the extracellular matrix (Chen *et al.* 2019), and promoting angiogenesis by upregulating VEGF-A during the inflammation phase (Shams *et al.* 2022). A study also showed that steroids and terpenes promote epithelialization, increase wound contraction, and increase collagenization. A recent study by (Fu *et al.* 2022) also reported glycosides phenylethanoid as the specific compound isolated from the *Paraboea rufescens*. In addition, glycosides play a role in terms of homeostasis and stimulation of granulation tissue (Nasa and Kumar 2020; Wu *et al.* 2020).

In this study, the antibacterial effects have been considered an important aspect of wound infection. Pathogenic bacteria such as *Staphylococcus aureus*, *Staphylococcus epidermidis*, and *Pseudomonas aeruginosa* have been investigated. The disc diffusion method showed that PGEE 2.5%, 5%, and 10% had inhibited bacterial growth. In contrast, the most inhibited was *S. epidermidis* compared to *S. aureus* or *P. aeruginosa* (Figure 1 and Supplementary Figure 3). The diameter of the inhibition zone ranged from 10.4

to 13, which was categorized as the strong inhibition activity (Puguh Surjowardojo and Tri Eko Susilorini 2015). However, *S. epidermidis* is a gram-positive bacteria with a simpler cell membrane that is easier to penetrate than a gram-negative bacteria. A study described that the antibacterial mechanism induced by a flavonoid compound was correlated with membrane plasma inhibition, impaired membrane permeability, and attenuated pathogenicity (Nanjala *et al.* 2022).

To evaluate the progress of wound healing effects, we observed that the full-thickness excision wound showed the wounds started to close after day 1 until day 12, even though there was no significant difference in the wound percentage among treatment groups (Figures 2A and B). Our result was in line with a study that the crude methanol extract of *Malva neglecta* has almost the same wound contraction as the standard and treatment groups. Furthermore, the higher concentration reduced wound diameter and was not significantly different from the positive control group (Saleem *et al.* 2020).

Several macrophages are also important to the wound-healing process. Based on the data from Figure 3 and HE images from Table 1, the bioplacenta group had the lowest number of macrophages compared to the other groups, followed by PGEE 10%. This result also aligned with the general theory that the number of macrophages will be high in the initial phase (1st week) and decrease over time in the second week of the injury. The results of this study are supported by the research of (Winarni *et al.* 2022), who used *Sargassum duplicatum* and *Garcinia mangostana* extracts to repair diabetic open wounds. In chronic wounds, proinflammatory macrophages persist without switching to an anti-inflammatory phenotype and interfere with tissue repair (Fedchenko and Reifenrath 2014; Krzyszczyk and 2018). Pro-wound healing macrophages produce growth factors such as PDGF, insulin-like growth factor-1 (IGF-1), VEGF, and TGF- β 1, which help cell proliferation, formation of granulation tissue, and angiogenesis (Murray and Wynn 2011; Vannella and Wynn 2017).

The application of PGEE is likely to affect the addition of nutrients to the wound area, which can optimize wound healing. The fibroblast decrease aligned with the collagen density score at PGEE 10%. In this case, fibroblasts were trans-differentiated more quickly into myofibroblasts for collagen synthesis on day 12, and the collagen formed at PGEE 10% also showed an increase (Figure 4 and 6). Fibroblasts are cells that play an important role in the proliferative

phase, which functions to regulate collagen, glycosaminoglycans, proteoglycans, fibronectin, and elastin as extracellular components (Wulandari *et al.* 2021). An increase in fibroblasts will accelerate the healing process in the inflammatory and proliferative phases (Maruf *et al.* 2021). While in the remodeling phase, it can be identified by decreased proliferation and inflammation, extracellular matrix assembly, and regression of newly formed capillaries. The proliferative phase can occur from the 4th to the 21st day after the wound starts, whereas the remodeling phase begins in the second week after the wound occurs, which causes the wound healing stages to overlap. At a certain point in the proliferative phase, apoptosis of fibroblast cells occurs when the collagen matrix has filled the wound cavity (Wong *et al.* 2013; Johnson and Wilgus 2014).

Blood vessels, as shown in Figure 5, are also important factors indicating that PGEE 2.5% was more than the other four groups and PGEE 10% was the lowest. Our result aligned with the general theory that blood vessels have begun to decrease in the healing phase, entering the remodeling phase, where the healing effect begins on day 12. This result was also supported by (Atik and Iwan 2009), that an increased number of fibroblasts, blood vessels, and the expression of VEGF-A in the proliferative phase were observed on the days fifth. On the other hand, the data shows that the number of blood vessels has decreased on the 12th day, which means that remodeling is the final phase after the final proliferation, which shows the number of cells involved (blood vessels, fibroblasts, and collagen) in the process of wound healing begins to decrease (Choudhary *et al.* 2020).

As presented in Table 1, tissue observation by histology images showed the different bundles of fine fibers with a bright pink streak marking the collagen (as indicated by the arrows). Collagen build-up has started to appear in all groups. The Bioplacenton group had denser collagen fibers than the other groups, followed by PGEE 5% and PGEE 10%. Unlike the negative control group, there was no visible collagen formation. Collagen deposition was higher in the skin applied to Bioplacenton, followed by the PGEE 5% and PGEE 10% groups, which were not too different, indicating a faster wound healing efficiency than the negative control group (Figure 6). The fiber density is not maximal yet, maybe because it is still in the transitional stage of collagen type III to collagen type I, which is still in the final proliferative

stage towards wound remodeling. In research by (Teng *et al.* 2022), there was a 1.6 times fold increase in collagen deposition on day 7 post-injury in the hucMSCs-exo (human umbilical cord mesenchymal stem cells) treated group. In the last stages, adequate collagen from type III to type I is deposited orderly, leading to tissue remodeling and wound repair. A study by (Addis *et al.* 2020) stated in their research that the phytochemical compounds in plants can stimulate collagen synthesis and cell proliferation activity, biological processes that are highly involved in wound healing. Phenolic compounds also mediate cell proliferation in injured tissue by increasing collagen synthesis and collagen maturation, which are associated with producing proinflammatory cytokines (Umar *et al.* 2020). Furthermore, collagen plays a key role in organogenesis and tissue regeneration (Sallehuddin *et al.* 2022).

The results of the VEGF data expressed by the IRS score in Figure 7 align with the general theory of wound healing. Bioplacenton, PGEE 5%, and PGEE 10% showed moderate expression of VEGF in the endothelial cells as well as Base gel, and PGEE 2.5% showed high expression in the vascular endothelial cells, fibroblast cells, and epithelial cells (Table 1 and Figure 7). Research by (Sunarto *et al.* 2020) evaluated the effect of a hypoxic conditional medium of mesenchymal stem cells (HMSCs-CM) on VEGF and collagen concentrations in rat incision wounds. VEGF levels increased significantly on day 6 in a dose-dependent manner. Interestingly, VEGF levels gradually decreased on day 9. In addition, the decrease in VEGF levels on day 9 in their study agreed with our findings, where we found a tendency to decrease collagen density, indicating the completion of the remodeling phase and accelerated wound healing. One of the VEGF mediators, nitric oxide (NO), increases collagen deposition in diabetic wounds by activating fibroblasts (Philip Bao 2009; Shams *et al.* 2022). Consistent with this mechanism, VEGF can promote healing on multiple levels. Although PDGF and TGF- β are efficacious on skin wounds, VEGF can stimulate additional components of wound healing independently of PDGF and TGF- β (Savari *et al.* 2019; Raina *et al.* 2021).

On the 12th day of observation (Table 1), the distribution of VEGF antibodies accumulated in the cytoplasm that diffused in the Bioplacenton group compared to the PGEE 10% were identical. The staining of brownish cobblestone was visibly reduced

or just slightly protein expression, which shows a concentration of PGEE 10% was able to produce wound healing effects. Thus, VEGF was expressed in capillary endothelial cells of new blood vessel walls and old blood vessels, as seen on slides stained with HE. VEGF is produced by many cell types, such as endothelial cells, fibroblasts, macrophages, smooth muscle cells, neutrophils, and platelets, which are functionally involved in wound healing (Philip Bao 2009; Komi *et al.* 2020). This factor is unmatched for its effects on various components of the wound repair cascade, such as angiogenesis, collagen deposition, and epithelialization (Shams *et al.* 2022).

Acknowledgements

Authors acknowledge the kind help and contributions of Primkoppol Puslabfor POLRI Jakarta Selatan, Herbarium Bogoriense, Laboratorium Pharmacology and Microbiology, and Laboratorium Histology, Faculty of Pharmacy, Universitas Sumatera Utara.

References

- Addis, R., Cruciani, S., Santaniello, S., Bellu, E., Sarais, G., Ventura, C., Pintore, G., 2020. Fibroblast proliferation and migration in wound healing by phytochemicals: evidence for a novel synergic outcome. *International Journal of Medical Sciences*. 17, 1030–1042. <https://doi.org/10.7150/ijms.43986>
- Aji, N., Rubiyanti, R., 2021. The potential of *Tradescantia spathaceae* leaves infusion as sunscreen gel use spectrophotometric UV-Vis method. *Jurnal Ilmu Kefarmasian Indonesia*. 20, 6–13.
- Atik, N., Iwan, A.R.J., 2009. Perbedaan efek pemberian topikal gel lidah buaya (*Aloe vera* L.) dengan solusi povidone Iodine terhadap penyembuhan luka sayat pada kulit mencit (*Mus musculus*). *Majalah Kedokteran Bandung*. 41, 29–36. <https://doi.org/10.15395/mkb.v41n2.188>
- Chen, Y., Tian, L., Yang, F., Tong, W., Jia, R., Zou, Y., Yin, Z., 2019. Tannic acid accelerates cutaneous wound healing in rats via activation of the ERK 1/2 signaling pathways. *Advances in Wound Care*. 8, 341–354. <https://doi.org/10.1089/wound.2018.0853>
- Choudhary, A., Kant, V., Jangir, B.L., Joshi, V.G., 2020. Quercetin loaded chitosan tripolyphosphate nanoparticles accelerated cutaneous wound healing in Wistar rats. *European Journal of Pharmacology*. 880, 173172. <https://doi.org/10.1016/j.ejphar.2020.173172>
- Depkes RI, K.K.R., 2016. *Farmakognosi dan Fitokimia*. Pusdik SDM Kesehatan, Kemenkes RI, Jakarta Selatan.
- Ditjen POM, D.R., 2000. *Parameter Standar Umum Ekstrak Tumbuhan Obat*, sixth ed. Departement Kesehatan Republik Indonesia, Jakarta.
- Farnsworth, N.R., 1966. Biological and phytochemical screening of plants. *Journal of Pharmaceutical Sciences*. 55, 225–276. <https://doi.org/10.1126/science.151.3712.874>
- Fedchenko, N., Reifenrath, J., 2014. Different approaches for interpretation and reporting of immunohistochemistry analysis results in the bone tissue - a review. *Diagnostic Pathology*. 9, 221. <https://doi.org/10.1186/s13000-014-0221-9>
- Fu, X., Chen, J., Xie, R., Zhou, L., Wei, Y., Yuan, C., Gu, W., 2022. Phytochemical and chemotaxonomic studies on *Paraboea rufescens* (Gesneriaceae). *Biochemical Systematics and Ecology*. 102, 104414. <https://doi.org/10.1016/j.bse.2022.104414>
- Gong, X., Xu, Y., Ren, K., Bai, X., Zhang, C., Li, M., 2019. Phenylethanoid glycosides from *Paraboea martinii* protect rat pheochromocytoma (PC12) cells from hydrogen peroxide-induced cell injury. *Bioscience, Biotechnology and Biochemistry*. 83, 2202–2212. <https://doi.org/10.1080/09168451.2019.1654359>
- Harahap, N.I., 2017. Uji Aktivitas Antibakteri Gel Ekstrak Etanol Daun Sambung Rambat (*Mikania micrantha* Kunth.) Terhadap Angiogenesis Luka Eksisi Terinfeksi Pada Marmut [Theses]. Medan, Indonesia: Institut Universitas Sumatera Utara.
- Johnson, K.E., Wilgus, T.A., 2014. Vascular endothelial growth factor and angiogenesis in the regulation of cutaneous wound repair. *Advances in Wound Care*. 3, 647–661. <https://doi.org/10.1089/wound.2013.0517>
- Komi, D.E.A., Khomtchouk, K., Santa Maria, P.L., 2020. A review of the contribution of mast cells in wound healing: involved molecular and cellular mechanisms. *Clinical Reviews in Allergy and Immunology*. 58, 298–312. <https://doi.org/10.1007/s12016-019-08729-w>
- Krzyszczczyk, P., Schloss, R., Palmer, A., Berthiaume, F., 2018. The role of macrophages in acute and chronic wound healing and interventions to promote pro-wound healing phenotypes. *Frontiers in Physiology*. 9, 1–22. <https://doi.org/10.3389/fphys.2018.00419>
- Maruf, M.T., Dewi, P.S., Nurlitasari, D.F., 2021. Efficacy of Bidara leaf (*Ziziphus mauritiana*) viscous extract to gingival wound healing in wistar rats. *Journal of International Dental and Medical Research*. 14, 1367–1372.
- Moieni, A., Pedram, P., Makvandi, P., Malinconico, M., Gomez d'Ayala, G., 2020. Wound healing and antimicrobial effect of active secondary metabolites in chitosan-based wound dressings: a review. *Carbohydrate Polymers*. 233, 115839. <https://doi.org/10.1016/j.carbpol.2020.115839>
- Murray, P.J., Wynn, T.A., 2011. Protective and pathogenic functions of macrophage subsets. *Nature Reviews Immunology*. 11, 723–737. <https://doi.org/10.1038/nri3073>
- Nanjala, C., Odago, W.O., Rono, P.C., Waswa, E.N., Mutinda, E.S., Oulo, M.A., Hu, G.W., 2022. A review on ethnobotany, phytochemistry, and pharmacology of the genus *Didymocarpus* wall. (Gesneriaceae). *Journal of Ethnopharmacology*. 295, 115404. <https://doi.org/10.1016/j.jep.2022.115404>
- Nasa, P., Kumar, H., 2020. Plants having wound healing property: a review. *J. Pharm. Sci. and Res*. 12, 1071–1075.
- Nurhayati, L.S., Yahdiyani, N., Hidayatulloh, A., 2020. Perbandingan pengujian aktivitas antibakteri starter yogurt dengan metode difusi sumuran dan metode difusi cakram. *Jurnal Teknologi Hasil Peternakan*. 1, 41. <https://doi.org/10.24198/jthp.v1i2.27537>
- Panche, A.N., Diwan, A.D., Chandra, S.R., 2016. Flavonoids: an overview. *Journal of Nutritional Science*. 5, 47. <https://doi.org/10.1017/jns.2016.41>
- Philip Bao, 2009. The role of vascular endothelial growth factor in wound healing. *J. Surg. Res*. 23, 1–7. <https://doi.org/10.1016/j.jss.2008.04.023>

- Puguh Surjowardojo, Tri Eko Susilorini, G.R.B.S., 2015. Daya hambat dekok kulit apel manalagi (*Malus sylvestris* Mill.) terhadap pertumbuhan *Staphylococcus aureus* dan *Pseudomonas* sp. penyebab mastitis pada sapi perah. *J. Ternak Tropika*. 16, 40–48.
- Purnomo, H., Syamsul, E.S., 2012. *Statistika Farmasi: Aplikasi Praktis dengan SPSS*. Grafika Indah, Yogyakarta.
- Raina, N., Rani, R., Gupta, M., 2021. Angiogenesis: aspects in wound healing, in: Chatterjee, S. (Eds.), *Endothelial Signaling in Vascular Dysfunction and Disease*. Academic Press, London, pp. 77–90. <https://doi.org/10.1016/B978-0-12-816196-8.00010-2>
- Saleem, U., Khalid, S., Zaib, S., Anwar, F., Ahmad, B., Ullah, I., Ayaz, M., 2020. Phytochemical analysis and wound healing studies on ethnomedicinally important plant *Malva neglecta* Wallr. *Journal of Ethnopharmacology*. 249, 112401. <https://doi.org/10.1016/j.jep.2019.112401>
- Sallehuddin, N., Fadilah, N.I.M., Hwei, N.M., Wen, A.P.Y., Yusop, S.M., Rajab, N.F., Fauzi, M.B., 2022. Characterization and cytocompatibility of collagen-gelatin-elastin (CollaGee) acellular skin substitute towards human dermal fibroblasts: *in vitro* assessment. *Biomedicine*. 10, 1–16. <https://doi.org/10.3390/biomedicine10061327>
- Sara Surya, Rosiana Rizal., 2021. Formulasi dan uji stabilitas fisik gel AHA (Alpha Hydroxy Acid) kombinasi BHA (Beta Hydroxy Acid) sebagai eksfolieting dalam penanganan melasma. *Syntax Literate: Jurnal Ilmiah Indonesia*. 6, 1–13.
- Savari, R., Shafiei, M., Galehdari, H., Kesmati, M., 2019. Expression of VEGF and TGF- β genes in skin wound healing process induced using phenytoin in male rats. *Jundishapur Journal of Health Sciences*. 11, 1–5. <https://doi.org/10.5812/jjhs.86041>
- Shah, A., Amini-Nik, S., 2017. The role of phytochemicals in the inflammatory phase of wound healing. *International Journal of Molecular Sciences*. 18, 1068. <https://doi.org/10.3390/ijms18051068>
- Shams, F., Moravvej, H., Hosseinzadeh, S., Mostafavi, E., Bayat, H., Kazemi, B., Moosavian, H., 2022. Overexpression of VEGF in dermal fibroblast cells accelerates the angiogenesis and wound healing function: *in vitro* and *in vivo* studies. *Scientific Reports*. 12, 1–15. <https://doi.org/10.1038/s41598-022-23304-8>
- Su, Z.L., Su, C.W., Huang, Y.L., Yang, W.Y., Sampurna, B.P., Ouchi, T., Yuh, C.H., 2019. A novel AURKA mutant-induced early-onset severe hepatocarcinogenesis greater than wild-type via activating different pathways in Zebrafish. *Cancers*. 11, 927. <https://doi.org/10.3390/cancers11070927>
- Sunariani, J., Rossa, L.M., Yuliati, Y., Diyatri, I., Juliastuti, W.S., Oki, A.S., 2020. Immunoreactive scoring of metallothionein-3 (MT-3) expression as an indicator of metallic taste rats which are induced by doxorubicin and antioxidant. *Malaysian Journal of Medicine and Health Sciences*. 16, 42–46.
- Sunarto, H., Trisnadi, S., Putra, A., Sa'dyah, N.A.C., Tjipta, A., Chodidjah, C., 2020. The role of hypoxic mesenchymal stem cells conditioned medium in increasing vascular endothelial growth factors (VEGF) levels and collagen synthesis to accelerate wound healing. *Indonesian Journal of Cancer Chemoprevention*. 11, 134. <https://doi.org/10.14499/indonesianjcanchemprev11iss3pp134-143>
- Suvarna, S.K., Layton, C., Bancroft, J.D., 2019. *Bancroft's theory and practice of Histological Techniques*. Elsevier, Nottingham. [https://doi.org/10.1016/s0031-3025\(16\)35811-1](https://doi.org/10.1016/s0031-3025(16)35811-1)
- Teng, L., Maqsood, M., Zhu, M., Zhou, Y., Kang, M., Zhou, J., Chen, J., 2022. Exosomes derived from human umbilical cord mesenchymal stem cells accelerate diabetic wound healing via promoting M2 macrophage polarization, angiogenesis, and collagen deposition. *International Journal of Molecular Sciences*. 23, 10421. <https://doi.org/10.3390/ijms231810421>
- Umar, T.P., Wijaya, F., Ernanto, J.H., Parulian, T., 2020. The effect of *Lansum domesticum* Corr. (Duku) seed extract on wound healing. *Journal of Nobel Medical College*. 9, 8–11. <https://doi.org/10.3126/jonmc.v9i1.29395>
- Vannella, K.M., Wynn, T.A., 2017. Mechanisms of organ injury and repair by macrophages*. *Annual Review of Physiology*. 79, 593–617. <https://doi.org/10.1146/annurev-physiol-022516-034356>
- Wang, X., Li, L., Bai, Z., Peng, Y., Xiao, P., Liu, Y., 2011. Five new phenylpropanoid glycosides from *Paraboea glutinosa* (Gesneriaceae). *Journal of Natural Medicines*. 65, 301–306. <https://doi.org/10.1007/s11418-010-0493-7>
- Winarni, D., Husna, F.N., Syadzha, M.F., Susilo, R.J.K., Hayaza, S., Ansori, A.N.M., Awang, K., 2022. Topical administration effect of *Sargassum duplicatum* and *Garcinia mangostana* extracts combination on open wound healing process in diabetic mice. *Scientifica*. 2022, 9700794. <https://doi.org/10.1155/2022/9700794>
- Winastri, N.L.A.P., Muliastri, H., Hidayati, E., 2020. Aktivitas antibakteri air perasan dan rebusan daun calincing (*Oxalis corniculata* L.) terhadap *Streptococcus mutans*. *Berita Biologi*. 19, 223–230. <https://doi.org/10.14203/beritabiologi.v19i2.3786>
- Wise, L.M., Stuart, G.S., Real, N.C., Fleming, S.B., Mercer, A.A., 2018. VEGF receptor-2 activation mediated by VEGF-E limits scar tissue formation following cutaneous injury. *Advances in Wound Care*, 7, 283–297. <https://doi.org/10.1089/wound.2016.0721>
- Wong, V.W., Gurtner, G.C., Longaker, M.T., 2013. Wound healing: a paradigm for regeneration. *Mayo Clinic Proceedings*. 88, 1022–1031. <https://doi.org/10.1016/j.mayocp.2013.04.012>
- Wu, L., Georgiev, M.I., Cao, H., Nahar, L., El-Seedi, H.R., Sarker, S.D., Lu, B., 2020. Therapeutic potential of phenylethanoid glycosides: a systematic review. *Medicinal Research Reviews*. 40, 2605–2649. <https://doi.org/10.1002/med.21717>
- Wulandari, P.A.C., Ilmi, Z.N., Husen, S.A., Winarni, D., Alamsjah, M.A., Awang, K., Pudjiastuti, P., 2021. Wound healing and antioxidant evaluations of alginate from sargassum ilicifolium and mangosteen rind combination extracts on diabetic mice model. *Applied Sciences*. 11, 4651. <https://doi.org/10.3390/app11104651>

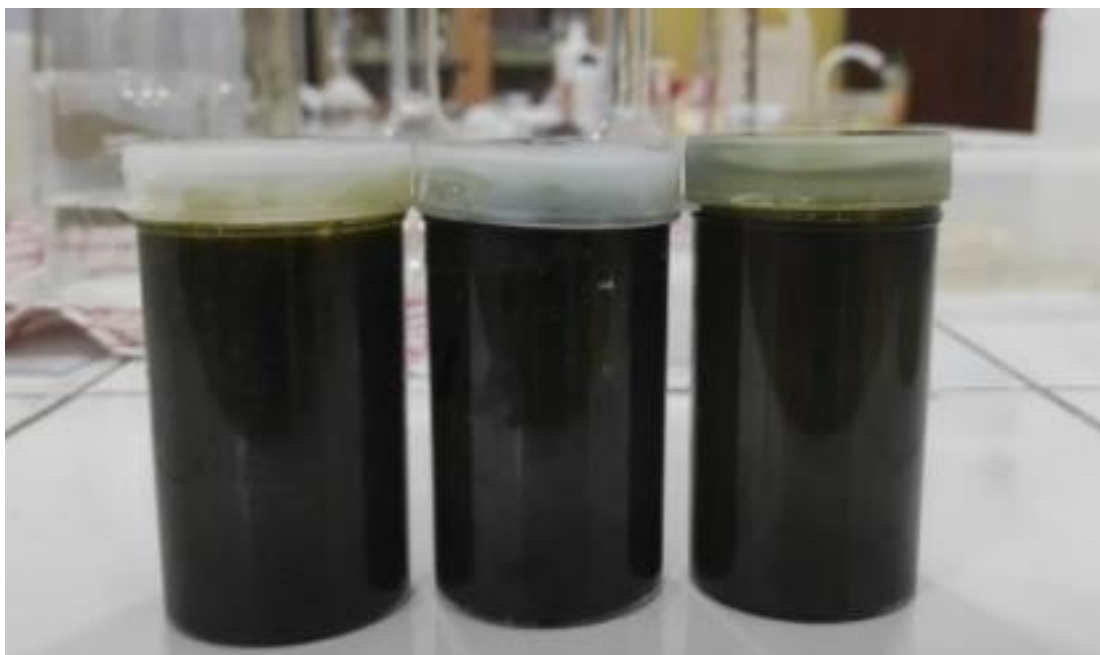
Supplementary Materials



Supplementary Figure 1. Plant identification of *Paraboea leuserensis*

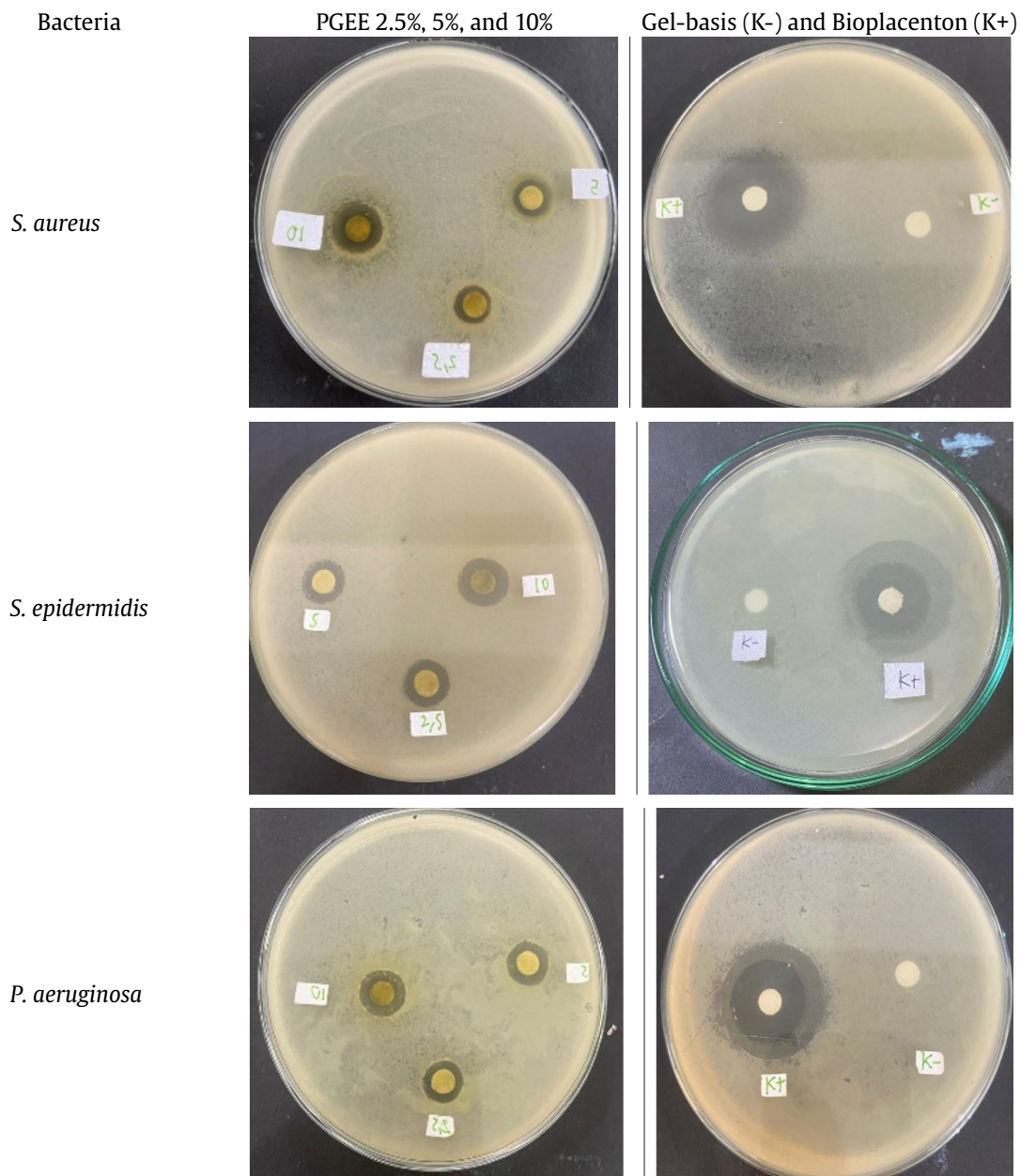


A



B

Supplementary Figure 2. (A) *Paraboa leuserensis* in crude extract and (B) the gel-based ethanolic extract or PGEE



Supplementary Figure 3. Disc diffusion photograph of PGEE 2.5%, 5% and 10% compared with Gel-basis (K-) and Bioplacenton (K+) against *S. aureus*, *S. epidermidis*, and *P. aeruginosa*

Supplementary Table 1. Physical stability of PGEE before and after cyclic test (CT)

Parameter	(2.5%)		(5%)		(10%)	
	Before CT	After CT	Before CT	After CT	Before CT	After CT
Organoleptic and Homogeneity	unique odor, dark green, viscous gel, homogeneous	unique odor, dark green, rather sticky gel, homogeneous	unique odor, dark green, rather sticky gel, homogeneous			
Viscosity (cp)	49021.3	8137.9	34490.6	7854.1	24798.4	5007.5
pH	6.43±0.06	6.40 - 6.32	6.38±0.06	6.38 - 6.30	6.36±0.06	6.35 - 6.28
Spread ability (cm)	0 gr: 3.6	0 gr: 4	0 gr: 3.8	0 gr: 4.3	0 gr: 4.0	0 gr: 4.5
	100gr: 3.9	100gr: 4.2	100gr: 4.1	100gr: 4.5	100gr: 5.2	100gr: 5.6
	125 gr: 4.2	125 gr: 4.4	125 gr: 4.4	125 gr: 4.7	125 gr: 5.7	125 gr: 6

Supplementary Table 2. Phytochemical screening by LC-MS/MS

Compounds	Formula	Molecular weight	RT [min]	Area[Max.]	mz cloud best match
Choline	C5H13NO	103.10002	1.030	3,279,846,535.08	97.5
Diisobutylphthalate	C16H22O4	278.15184	18.506	654,653,590.93	99.2
Betaine	C5H11NO2	117.07921	1.086	331,012,330.41	95.0
Betaine	C5H11NO2	117.0792	0.977	327,764,872.03	95.0
NP-020014	C15H26O3	276.1725	13.937	251,017,055.52	66.4
2,2,6,6-Tetramethyl-1-piperidinol (TEMPO)	C9H19NO	157.1467	12.788	238,837,378.17	93.8
Quercetin	C15H10O7	302.04256	8.125	218,365,277.43	99.7
N4-(3-Methyl-4-nitroisoxazol-5-yl)-3-(2,6-dichlorophenyl)-5-methylisoxazole-4-carboxamide	C15H10Cl2N4O5	396.00977	1.048	178,196,779.69	65.1
Trigonelline	C7H7NO2	137.04779	0.979	176,860,705.62	99.4
Stearamide	C18H37NO	283.28737	24.585	156,217,103.20	97.4
2-(3,4-dihydroxyphenyl)-5,7-dihydroxy-3-[[[(2S,3R,4R,5R,6S)-3,4,5-trihydroxy-6-methyloxan-2-yl]oxy]-4H-chromen-4-one	C21H20O11	448.10065	8.126	150,175,886.20	98.4
1-[2-[(2,4-dichlorophenyl)sulfonyl]ethyl]-5-(trifluoromethyl)-2,3-dihydro-1H-1,4-diazepine	C14H13Cl2F3N2O2S	400.00472	1.118	118,173,138.64	66.2
5-Hydroxymethyl-2-furaldehyde	C6H6O3	126.03189	1.172	111,161,811.32	88.2
Palmitic acid	C16H32O2	273.26683	15.486	110,085,125.24	82.8
Quercetin	C15H10O7	132.04346	0.847	99,449,984.89	98.1
2-Amino-1,3,4-octadecanetriol	C18H39NO3	317.29302	18.722	99,377,881.75	66.7
1-(4-fluorophenyl)-2-[[4-methyl-5-(2-methyl-1,3-thiazol-4-yl)-4H-1,2,4-triazol-3-yl]thio]ethan-1-one	C15H13FN4OS2	348.04606	1.062	94,345,851.53	84.2
Stearamide	C18H37NO	283.28737	24.246	87,757,665.51	97.7
Ethyl palmitoleate	C18H34O2	282.2561	0.891	82,883,804.06	85.6
Ellagic acid	C14H6O8	302.00627	7.248	79,509,340.55	96.5
5-Hydroxymethyl-2-furaldehyde	C6H6O3	126.03189	1.512	77,160,021.60	92.0
Bis(4-ethylbenzylidene)sorbitol	C24H30O6	414.20482	15.154	76,742,621.69	99.2
Erucamide	C22H43NO	337.33446	25.661	74,783,108.73	94.9
2-[2-(5-bromo-2-pyridyl)diaz-1-enyl]-5-(diethylamino)phenol	C15H17BrN4O	348.06133	1.008	65,788,178.33	67.9
Hexadecanamide	C16H33NO	255.25627	21.600	61,364,592.28	98.8
Azithromycin impurity A	C37H70N2O12	1469.00522	1.022	61,181,560.39	66.4
Cetrimonium	C19H41N	283.32402	20.287	55,788,014.63	97.3
acridine-9(10H)-thione	C13H9NS	211.04578	17.803	53,365,449.90	96.9
n-Pentyl isopentyl phthalate	C18H26O4	323.20979	18.489	52,181,134.61	83.0
7-Hydroxycoumarine	C9H6O3	162.03172	10.611	49,535,871.30	89.5
2-Amino-1,3,4-octadecanetriol	C18H39NO3	317.29302	15.638	46,519,312.33	81.2
Hexadecanamide	C16H33NO	255.25627	22.633	46,291,299.88	97.4
2-(3,4-dihydroxyphenyl)-5,7-dihydroxy-3-[[[(2S,3R,4R,5R,6S)-3,4,5-trihydroxy-6-methyloxan-2-yl]oxy]-4H-chromen-4-one	C21H20O11	448.10082	0.844	44,167,847.52	96.6
Diisobutylphthalate	C16H22O4	278.15187	18.630	41,640,623.59	99.2
5-Hydroxymethyl-2-furaldehyde	C6H6O3	126.03187	1.772	40,810,219.91	92.0
Hexadecanamide	C16H33NO	255.25627	22.332	40,220,003.81	99.3
1-[2,6-dichloro-4-(trifluoromethyl)phenyl]-3-methyl-1H-pyrazole-4,5-dione 4-(N-phenylhydrazone)	C17H11Cl2F3N4O	381.99418	0.975	39,874,042.05	63.0
Trigonelline	C7H7NO2	155.05836	0.866	38,851,968.48	85.6
Monobutylphthalate	C12H14O4	222.0894	18.487	36,830,330.97	96.3
Oleamide	C18H35NO	281.27193	22.151	36,101,868.54	96.8

Supplementary Table 2. Continued

Compounds	Formula	Molecular weight	RT [min]	Area[Max.]	mz cloud best match
(2S,3R,4S,5S,6R)-3,4,5-trihydroxy-6-(hydroxymethyl)oxan-2-yl(2E)-3-phenylprop-2-enoate	C15H18O7	332.08721	7.638	35,454,158.38	97.6
Tributyl phosphate	C12H27O4P	266.16488	17.067	34,503,418.93	99.8
Ethyl palmitoleate	C18H34O2	282.256	22.79	32,320,338.44	81.9
Palmitic acid	C16H32O2	273.26683	15.895	31,795,658.84	62.3
D-(+)-Proline	C5H9NO2	115.06358	1.092	30,218,660.17	91.6
Oleoyl ethanolamide	C20H39NO2	307.28749	22.477	28,995,405.23	66.5
D-(+)-Proline	C5H9NO2	115.06358	0.971	27,498,423.12	99.2
Ellagic acid	C14H6O8	302.00627	6.059	26,361,455.29	97.4
Stearoyl Ethanolamide	C20 H41 N O2	309.30297	23.878	25,823,649.03	85.4
3,5-di-tert-Butyl-4-hydroxybenzaldehyde	C15H22 O2	234.1621	17.558	25,192,800.80	98.7
α -Eleostearic acid	C18H30 O2	278.22469	20.127	24,481,360.59	93.3
3-(4-Chloro-3-methylphenyl)-7-(trifluoromethyl)-2,3-dihydrobenzol[4,5]imidazo[2,1-b][1,3]thiazol-3-ol	C17H12OIF3N2OS	384.02925	1.203	24,395,401.59	81.5
4-[(4-chlorophenyl)thio]-1-methyl-1H-pyrazolo[3,4-d]pyrimidine	C12H9CIN4S	276.02721	6.448	24,306,104.24	80.0
Dibenzylamine	C14H15N	197.12062	7.775	24,123,319.51	97.5
Stearoyl Ethanolamide	C20 H41 N O2	309.30297	23.279	23,689,394.45	84.8
1-(4-fluorophenyl)-2-[[4-methyl-5-(2-methyl-1,3-thiazol-4-yl)-4H-1,2,4-triazol-3-yl]thio]ethan-1-one	C15H13FN4OS2	348.04606	0,981	23,368,339.23	84,2
L-Pyroglutamic acid	C5H7NO3	129.04277	1.134	22,262,750.20	94.1
Erucamide	C22H43NO	337.33446	26.296	21,764,068.74	97.0
2-Amino-1,3,4-octadecanetriol	C18H39NO3	317.29302	19.134	19,180,033.69	80.8
4-amino-2-(4-chlorophenyl)-6-(methylthio)pyrimidine-5-carbonitrile	C12H9CIN4S	276.02712	0.845	18,777,450.97	72.9
Caprolactam	C6H11NO	113.08431	0.848	18,576,844.56	95.4
L{+}Arginine	C6H14N4O2	174.1118	1.071	18,461,835.33	71.9
Stearamide	C18H37NO	283.28737	25.336	16,725,813.01	97.4
Myricitrin	C21H20O12	464.09596	7.283	16,137,956.71	80.2
Tetranor-12(S)-HETE	C16H26O3	248.17772	17.557	16,095,008.40	74.3
α -Linolenic acid	C18H30O2	278.22469	20.586	14,789,138.07	93.6
Erucamide	C22H43NO	337.33446	26.135	14,696,555.03	97.0
7-Hydroxycoumarine	C9H6O3	162.03172	15.414	14,392,451.23	88.3
Bis(4-ethylbenzylidene)sorbitol	C24H30O6	414.20479	15.372	14,121,787.17	99.2
Stearoyl Ethanolamide	C20H41NO2	309.30297	25.814	14,062,643.89	92.4
2,2,6,6-Tetramethy-1-piperidinol (TEMPO)	C9H19NO	157.1467	0.957	13,727,839.90	93.0
Eicosapentaenoic acid	C20H30O2	308.23509	21.149	13,512,291.87	71.1
Myricetin	C15H10O8	318.03789	7.277	12,758,981.98	99.5
2-(Methylthio)benzothiatole	C8H7NS2	181.00214	14.554	12,729,373.90	97.8
2-Hydroxycinnamic acid	C9H8O3	146.03685	4.898	12,203,908.48	61.6
NP-011548	C18H34O3	280.24018	21.592	11,368,173.36	81.2
4-[(4-chlorophenyl)thio]-1-methyl-1H-pyrazolo[3,4-d]pyrimidine	C12H9CIN4S	276.02721	5.733	11,180,401.11	80.5
DEET	C12H17NO	191.13103	12.144	11,019,749.41	98.4
3,4-Dihydroxy phenylpropionic acid	C9H10O4	164.04746	13.964	10,959,207.77	89.6
N'-[6-[(5-chloro-3-pyridyl)oxy]-3-pyridyl]-N,N-dimethyliminoformamide	C13H13CIN4O	276.08223	1.092	10,695,415.54	90.4
Quercetin-3 β -D-glucoside	C21H20O12	464.09596	7.465	10,309,854.20	98.0

Supplementary Table 2. Continued

Compounds	Formula	Molecular weight	RT [min]	Area[Max.]	mz cloud best match
5-[4-(diethylamino)phenyl]-3-[(2-pyridin-2-ylethyl)amino]cyclohex-2-en-1-one	C21H25N3O	335.19985	7.709	10,118,121.36	61.5
Trilobutyl phosphate	C1242704P	266.1649	17.279	10,041,377.04	99.7
1-Stearoylglycerol	C21H42O4	358.30824	23.370	9,848,878.60	79.7
Sedanolide	C12H18O2	176.2012	20.334	9,718,873.34	76.8
PEG n5	C10H22O6	238.14173	0.885	9,627,061.22	86.8
Lorazepam	C15H10Cl2 N2O2	320.01717	5.734	9,621,351.24	65.0
Stearamide	C18H37NO	283.28737	22.912	9,287,149.63	93.8
Leucine	C6H13NO2	131.09477	0.956	9,207,971.38	81.6
1-Stearoylglycerol	C21H42O4	358.30824	22.778	8,452,561.83	94.7
5-Hydroxymethyl-2-furaldehyde	C6H6O3	126.03187	1.360	8,322,494.12	86.9
N,N-Dimethyldecylamine N-oxide	C12H27NO	201.20937	12.747	8,043,152.23	78.3
N'-(6-[(5-chloro-3-pyridyl)oxy]-3-pyridyl)-N,N-dimethyliminoforamamide	C13H13ClN4 O	276.08223	0.979	7,981,770.16	90.4
Sphingosine (d18:1)	C18H37NO2	321.26692	20.557	7,041,501.55	80.0
2-(14,15-Epoxyeicosatrienoyl) glycerol	C23H38O5	376.25902	20.464	6,568,547.93	92.3
Kaempferol	C15H10O6	286.04784	8.843	6,231,657.95	99.6
2-Hydroxycinnamic acid	C9H8O3	146.03685	10.983	5,412,233.26	60.3
Betaine	C5H11NO2	117.07921	26.359	4,768,404.23	93.7
Cyclohexylamine	C6H13N	99.10511	27.626	2,880,609.61	71.4